Directing Reaction Pathways on Supported Metal Catalysts with Low-Density Self-Assembled Monolayers

*Zachary Blanchette, Daniel K. Schwartz, and J. Will Medlin**

Department of Chemical and Biological Engineering, University of Colorado – Boulder, Boulder, Colorado 80309, United States

KEYWORDS: heterogeneous catalysis, surface modification, self-assembled monolayers, thiols, selectivity

ABSTRACT

Controlling reactant adsorption on catalyst surfaces is crucial to reaction activity and selectivity. One method for improving selectivity is by imposing steric constraints to bias the reactant binding orientation. In this study, thiol self-assembled monolayers (SAMs) were deposited onto Pt/Al_2O_3 catalysts as a method for controlling activity and selectivity via steric effects. In addition to a full monolayer, a low-density SAM-coated catalyst was employed. A number of characterization techniques demonstrated the successful deposition of homogeneous low-density SAMs on the

metal surface with reduced site-blocking compared to a full high-density monolayer. Reaction kinetic studies showed increased benzyl alcohol hydrodeoxygenation (HDO) selectivity for both SAM-modified catalysts. This was attributed to the inability of the reactant to adsorb on the catalyst with the aromatic ring parallel to the surface, thus preventing decarbonylation and ring hydrogenation reaction pathways. Additionally, SAM density influenced reaction activity significantly, with the low-density modified SAM catalyst being more active than the catalyst coated with a full monolayer. Moreover, liquid-phase hydrogenation reactions were used to investigate the relationship between SAM density and reactivity for reactant molecules of various sizes. In all cases, the low-density SAM improved reaction rates relative to dense SAMs. The effect of controlling ligand density depended on the type of reaction: high ligand densities greatly diminished ring hydrogenation while HDO was largely unaffected, suggesting a potential strategy for size-selective reaction rate and selectivity control.

1. Introduction

Organic ligands play an important role in the synthesis and modification of catalysts. Ubiquitous in the field of homogeneous catalysis, ligands are found in the structure of organometallic compounds that catalyze many important reactions. However, heterogeneous catalysts are often preferred due to their high thermal stability and ease of separation after reaction.[1,2] Heterogeneous catalysts are modified using many traditional methods to alter activity and selectivity including the synthesis of bifunctional catalysts containing two or more distinct sites working in tandem,[3,4] precisely controlling metal nanoparticle size,[5,6] or alloying multiple metals.[7,8] Furthermore, organic ligands can play an important role in the synthesis and functionalization of heterogeneous catalysts.

Ligands are often incorporated during the synthesis procedure of dispersed nanoparticle catalysts[9,10] or used to grow metal oxides, generating inverted metal/metal oxide catalysts.[11] Interestingly, organic ligands have been found to directly influence the catalytic behavior of metals through a variety of different mechanisms. Attaching organic ligands to a metal catalyst has been shown to alter electronic properties of the metal by changing the electron density of the metallic active site.[12,13] Ligands can also be used to provide additional functionality at an active site as seen in phosphonic acid-modified supported metal catalysts in which added Brønsted acidity from the SAM can improve hydrodeoxygenation rates,[14] or in the case where an amine can be incorporated into the tail of the SAM, offering additional reactant stabilization during CO_2 reduction.[15] The ligand moiety has been shown to specifically orient reactant molecules through intermolecular hydrophobic interactions[16] or aromatic stacking[17] to greatly improve reaction selectivity, conceptually similar to molecular recognition that is seen in many enzymes.[18] Finally, steric effects can greatly influence catalytic behavior by blocking active sites or restricting binding orientations responsible for certain reaction pathways.[19–21]

Of course, modifying catalysts with organic ligands is not without limitations. Ligands for heterogeneous catalyst modification are often in the form of self-assembled monolayers, which, in general, are dense and highly ordered. For this reason, improvements in selectivity are often accompanied by losses in overall activity due to significant site blocking.[22,23] Therefore, it is of considerable interest to generate ligand-modified catalysts with controlled surface densities in order to free active sites and restore activity while still gaining selectivity benefits from any of the reasons discussed above. Indeed, some examples in literature can be found addressing this issue. One method has been to restrict SAM coverage to specific locations on the catalyst surface.[23,24] In particular, the use of selective poisoning for surface molecular imprinting has been shown to

generate active islands related to the size and shape of the templated molecule resulting in imprinted Pd catalysts with high selectivity for hydrogenations of aromatic reactants.[21] Thiol coverage on Au clusters has been controlled through electric potential cycling or rigorous calcination steps to partially remove ligands.[25,26] While these methods result in lower ligand densities, they are not ideal if one wishes to maintain the integrity of the SAMs and prevent metal sintering. Finding a method for controlling SAM density that avoids harsh conditions and results in a consistent homogeneous SAM layer could have a significant effect on the use of organic ligands as a catalyst modification technique.

Several methods have been employed to generate "low-density" SAMs on metal films for various applications. For example, SAMs with submonolayer coverages have been prepared by precisely controlling the immersion conditions during deposition for very short times or using ultra-dilute concentrations.[27] However, due to the mechanism of SAM growth in which ligands deposit in a disordered state followed by nucleation and growth of ordered clusters, this may result in phase segregation in which there are islands of well-packed ligands and other areas with no ligands at all.[27,28] Depositing SAM layers using two or more different adsorbates has been demonstrated to influence ligand coverage but this method may also result in similar phase segregation issues and challenges in controlling the packing density or composition.[29] The use of chelating adsorbates has been shown to produce homogeneous monolayers with low tail density.[30,31] However, these SAMs still have a high surface density, limiting this method's potential for catalyst modification because a significant portion of active sites will be blocked. One promising technique to form low-density SAMs involves the deposition of ligands containing a bulky end-group followed by removal of that group after monolayer formation. This method has been shown to produce homogeneous low-density SAMs with potentially tunable gap sizes.[32–34]

In this work, we have adopted a synthesis technique developed by Olivier et al. with minor modifications as shown in Scheme 1.[35–37] This method for creating low-density thiol SAMs involved an ion exchange between 16-mercaptohexadecanoic acid (MHDA) and tetraethylammonium (TEA) to produce ligands with a sulfur headgroup and a large, bulky terminal group. These ligands were deposited onto Pt/Al_2O_3 where they bound to Pt through the sulfhydryl moiety. An additional ion exchange step was performed to remove TEA, resulting in a dispersed layer of MHDA. This method for low-density SAM formation offered several benefits compared to alternative strategies. First, this method has been shown to produce homogeneous SAM layers as opposed to phase segregated layers in which separate domains with different ligand densities coexist. Additionally, this approach is performed at ambient laboratory conditions, not only making it a simple, easily reproducible procedure, but avoiding harsh conditions such as high temperatures or shifting electric potentials that could damage the integrity of the catalyst (e.g., by causing sintering). We investigated the structure of these layers using a variety of characterization techniques, indicating successful deposition of homogeneous low-density SAMs on Pt/Al_2O_3. Reaction tests highlight the effects of steric hinderance provided by the SAMs to direct adsorbate orientations and limit reactions of large molecules, resulting in significant differences in catalytic selectivity and activity.

Scheme 1. Synthesis procedure of low-density SAMs

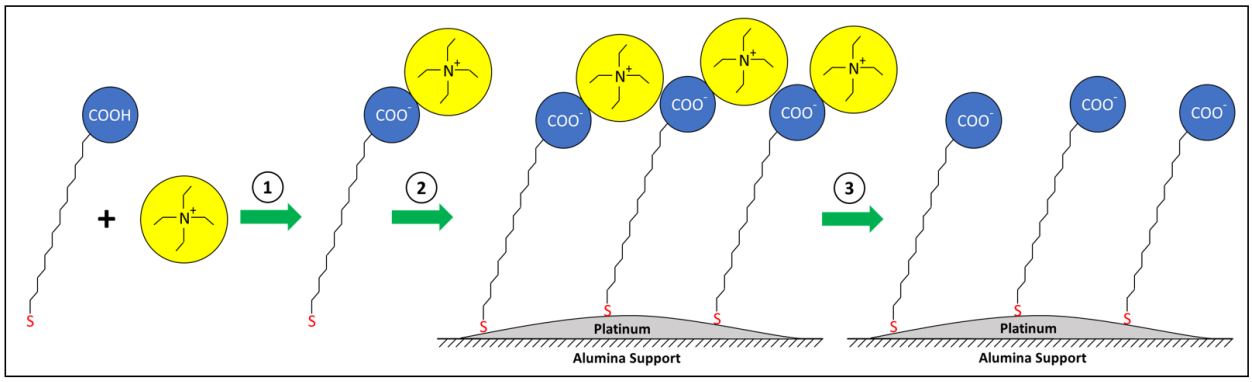

Footnote: Schematic diagram detailing the synthesis of low-density SAMs. Ion exchange is performed between 16-mercaptohexadecanoic acid (MHDA) and tetraethylammonium (TEA) resulting in an ion-pair. This ion-pair is then deposited onto the Pt/Al_2O_3 catalyst and additional ion exchange is performed to remove the bulky TEA resulting in a dispersed layer of MHDA.

2. Experimental Section

2.1 Materials

Benzyl alcohol (BZA, ≥ 99.0%), Pt/Al_2O_3 (5 wt% Pt), potassium perchlorate ($KClO_4$, ≥ 99.99%), tetraethylammonium hydroxide solution (TEAOH, 35 wt% in H_2O), 16-mercaptohexadecanoic acid (MHDA, 90%), carbon tetrachloride (CCl_4, 99.9%), 2-phenyl-2-butanol (99%), diphenylmethanol (99%), and decahydronaphthalene mixture of cis + trans isomers (decalin, ≥ 99%) were purchased from Sigma Aldrich. Silicon(IV) oxide (SiO_2, 99.9%) and n-heptadecane (99%) were purchased from Alfa Aesar. Dimethyl sulfoxide (DMSO, 99.9%) was purchased from Fisher Chemical. Anhydrous ethanol (200 proof) was obtained from Decon Laboratories, Inc. Ultrahigh-purity H_2, He, and N_2 were purchased from Airgas.

2.2 Catalyst Preparation

Full monolayer thiolate SAMs were prepared by depositing 150 mg of $5\%Pt/Al_2O_3$ catalyst powder in a 40 mL solution of 1 mM 16-mercaptohexadecanoic acid/carbon tetrachloride for 16 h. The supernatant was then decanted and the catalyst was washed with 40 mL of ethanol, which

was then poured off. 40 mL of fresh ethanol was added to the catalyst which was then vortex mixed and allowed to sit for 4 h. Again, the supernatant was decanted and the sample was washed with 40mL of fresh ethanol two more times. These washes consisted of adding ethanol to the catalyst and vortex mixing followed by centrifugation and decantation. Finally, the catalyst was dried in a room-temperature desiccator overnight. This procedure resulted in a full monolayer of MHDA on the 5%Pt/Al_2O_3 catalyst, hereafter referred to as "MHDA/5%Pt/Al_2O_3."

Low-density thiolate SAMs preparation was based on prior work for deposition of these LD-SAMs onto gold thin films shown in Scheme 1.[35–37] First, a solution of 1 mM 16-mercaptohexadecanoic acid and 6 mM tetraethylammonium hydroxide in carbon tetrachloride was prepared and allowed to equilibrate for 48 h to facilitate ion exchange between the anionic thiol and cationic tetraethylammonium. The resulting ion-pair thiol was then deposited onto 5%Pt/Al_2O_3 using the same technique as for the full monolayer described above. After the final ethanol wash, the catalyst was deposited into a 10 mM solution of $KClO_4$/DMSO for 16 h for additional ion exchange to remove the TEA counterion. Afterwards, the same ethanol washing and desiccation procedure was performed as for the full monolayer material. The finished material consisted of a low-density monolayer of MHDA on 5%Pt/Al_2O_3, hereafter referred to as "LD-MHDA/5%Pt/Al_2O_3."

Prior to characterization or use in any reaction, the modified catalyst samples were reduced in 40% H_2 at 250 °C for 1h and purged in helium or nitrogen as the sample cooled to room temperature.

2.3 Material Characterization

Diffuse reflectance infrared Fourier transform (DRIFT) spectra were obtained using a Thermo Fisher Scientific Nicolet 6700 FTIR using 100 scans at a 4 cm^{-1} resolution. CO DRIFTS was

performed using the same instrumentation equipped with a reaction chamber. The samples were first purged in a stream of argon for 30 min. CO was then dosed onto the sample for 20 min followed by another argon purge for 20 min before scanning. All DRIFTS experiments were performed at room temperature (~20 °C). Spectra of the samples prior to CO dosing was used as the background and subtracted to produce the reported spectra. Benzyl alcohol DRIFTS was performed using a similar procedure. Argon was bubbled through benzyl alcohol at room temperature to dose the pretreated catalysts held at 30 °C for 20 min. This was followed by an argon purge for 30 min before scanning. Spectra of the unmodified 5%Pt/Al_2O_3 sample prior to dosing was used as the background to produce the reported spectra.

Elemental composition was measured by inductively coupled plasma optical emission spectroscopy (ICP-OES). Samples were first digested in a mixture of HF/H_3PO_4/HCl/HNO_3 complexed with boric acid using a CEM Corp. Discover SP-D 80 digester. Samples were then analyzed using a Perkin Elmer Avio 500 inductively coupled optical emission spectrometer. Calibration was done using certified standards and Pt and S wt% were calculated using the average ICP results from triplicate catalyst batches.

CO chemisorption was performed using a Quantachrome Instruments Autosorb-1-C apparatus. Prior to measurements, 100 mg of pre-reduced sample was pretreated by heating to 200 °C for 3 h under vacuum. The treated sample was then cooled to 30 °C and the combined (physisorption plus chemisorption) isotherm was measured with a CO pressure of 100-400 mmHg and an equilibration time of 2 min. Platinum dispersion was determined by extrapolation to P=0. A Pt/CO stoichiometric ratio of 1 was used for calculating apparent dispersion, as suggested in literature for supported Pt catalysts.[38,39] Additionally, CO DRIFTS experiments revealed that the majority of

bound CO exists at peak locations corresponding to linearly bound CO, further validating this assumption.

X-ray photoelectron spectroscopy (XPS) was performed using a Kratos AxisSupra$^+$ XPS system with an Al K-α_1 x-ray source. Analysis was performed using CasaXPS software. Charge correction was performed by normalizing carbon 1s peak locations to 285.0 eV and peak fitting was done using a Shirley baseline. Peak locations and shifts were calculated using the average of two separate XPS experiments.

Transmission electron microscopy (TEM) images were obtained using a Tecnai ST20 with a LaB_6 electron gun operated at 160 kV. TEM samples were prepared by suspending pretreated catalyst particles in 5 mL of ethanol that was drop cast onto an ultrathin carbon film on a lacey carbon support film TEM grid. Average metal nanoparticle size was calculated from TEM images of 160 particles. Error was estimated using the standard deviation of average particle size separated in subsets of 20 particles.

2.4 Reaction Studies

Catalysts were tested for gas-phase benzyl alcohol hydrogenation using a tubular packed bed flow reactor. The reaction pathways are shown in Figure 1a. The reactor temperature was 177 °C and the reactions were performed at atmospheric pressure. Helium was bubbled through the liquid reactant (benzyl alcohol) held at 53 °C. This stream then merged with H_2 and additional make-up helium before reaching the catalyst bed giving a total flowrate of 160 sccm and final gas-phase mole fractions of Y_{H2} = 25% and Y_{BZA} = 0.053%. The reactor effluent was analyzed using an Agilent 7890A Gas Chromatograph equipped with an Agilent HP-5 capillary column and flame

ionization detector. Comparisons to retention times of known samples were used to confirm the products. Catalyst loading was controlled to obtain conversions of 8 ± 2%.

Liquid-phase hydrogenation reactions of benzyl alcohol (Figure 1a), 2-phenyl-2-butanol (Figure 1b), and diphenylmethanol (Figure 1c) were performed in a 50 mL Parr semibatch reactor. The reactor contained 20 mL of decalin solvent, 0.1 M n-heptadecane as an internal standard, and a known concentration of the reactant, which varied depending on the reactant used. Hydrogen pressure was maintained at 500 psi. The stir rate was kept at approximately 900 RPM and the reactions ran for 1 h. Other reaction conditions were varied depending on the reactant and are shown in Table S1. After a defined reaction time, a liquid sample of approximately 1 mL was withdrawn from a disposable filter attached to the reactor. Liquid samples were then analyzed using the same Agilent 7890A Gas Chromatograph. The majority of products were identified through comparison to retention times of known samples. Products from the ring hydrogenation of diphenyl methanol were determined via GC-MS analysis using a Thermo ISQ single quadrupole mass spectrometer coupled to a ThermoFisher Scientific TRACE 1310 gas chromatograph equipped with a Phenomenex Zebron ZB-5HT Inferno column analyzed using Chromeleon 7.2 SR4 with an embedded MS library. The ring hydrogenation product from the reaction of 2-phenyl-butanol (2-cyclohexyl-2-butanol) was also determined using the same GC-MS system. Analysis of the mass spectra, shown in Figure S1, did not provide a good match to any compounds in the spectral library. However, the product was determined through manual analysis of the spectra as discussed in the supporting information.

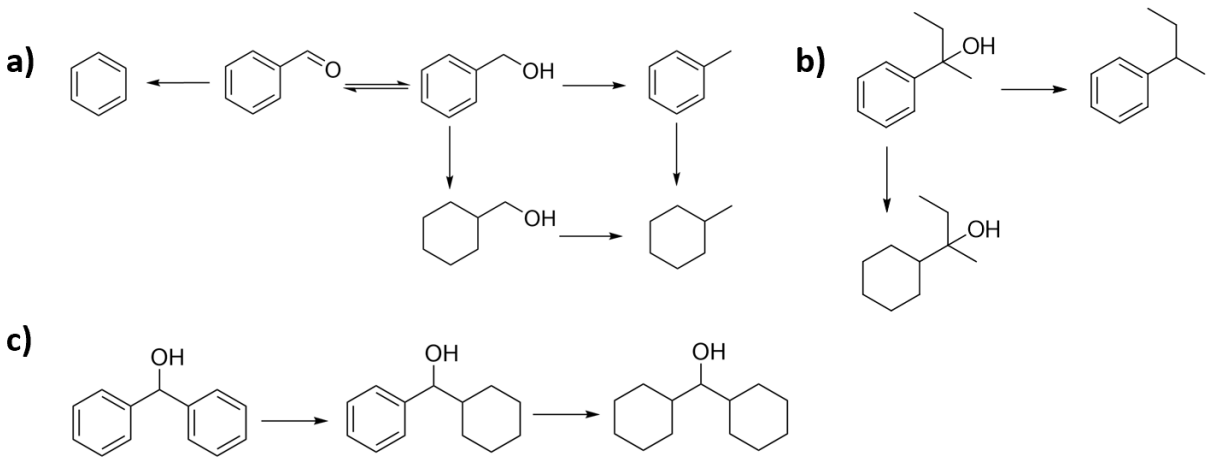

Figure 1. Reaction pathways for hydrogenations of reactants used in this study. a) Benzyl alcohol, b) 2-phenyl-2-butanol, and c) diphenylmethanol.

3. Results and Discussion

3.1 Characterization

The density of 16-mercaptohexadecanoic acid (MHDA) ligands on 5%Pt/Al_2O_3 was controlled to examine the benefits of a low-density monolayer compared to a full monolayer and an unmodified catalyst. Shown in Scheme 1, low-density SAMs were generated through an ion exchange process utilizing anionic MHDA and cationic tetraethylammonium (TEA) to create a ligand with a bulky terminal group. After deposition onto Pt/Al_2O_3, additional ion exchange was performed to remove TEA resulting in a film of MHDA with sub-monolayer coverage.[35–37] It was hypothesized that a full monolayer of MHDA would alter reaction selectivity through steric effects imposed by the ligands. However, full monolayers are thought to block a significant portion of active sites, limiting overall activity. Catalysts prepared with a low-density SAM may in some cases maintain selectivity benefits while partially restoring activity due to reduced site blocking.

DRIFT spectra shown in Figure 2a provide evidence that SAMs were successfully deposited onto 5%Pt/Al_2O_3. Focusing on the C-H stretching region, no peaks were found on the unmodified sample. In contrast, methylene stretches were clearly observed for both coated samples indicating successful deposition. In addition to confirming the presence of the SAMs, the relative peak locations and sizes provided insight into the ordering and concentration of ligands. For MHDA/5%Pt/Al_2O_3, antisymmetric and symmetric methylene stretches occurred at 2924.5 cm^{-1} and 2853.9 cm^{-1} respectively. Meanwhile, these stretches occurred at 2926.8 cm^{-1} and 2857.0 cm^{-1} for LD-MHDA/5%Pt/Al_2O_3. This shift to higher wavenumbers indicated greater disorder, as would be expected for a low-density SAM.[30,40–42] Additionally, the relative peak intensities were smaller for LD-MHDA/5%Pt/Al_2O_3, a result of a lesser number of thiols on the surface. A small shoulder at approximately 2960 cm^{-1} can also be seen for both modified samples, possibly a C-H methyl stretch from impurities in the thiol. Given that the spectra suggested the existence of well-defined SAMs, it is inferred that the SAMs were stable after the pretreatment at 250 °C and therefore should also be stable under the milder reaction conditions. Additional DRIFT spectra, shown in Figure S2, were obtained for catalysts aged in ambient storage conditions over the course of 30 days. There was little difference in peak shape or location with time, indicating that these SAMs were stable for at least 30 days. All samples were used within 30 days of synthesis.

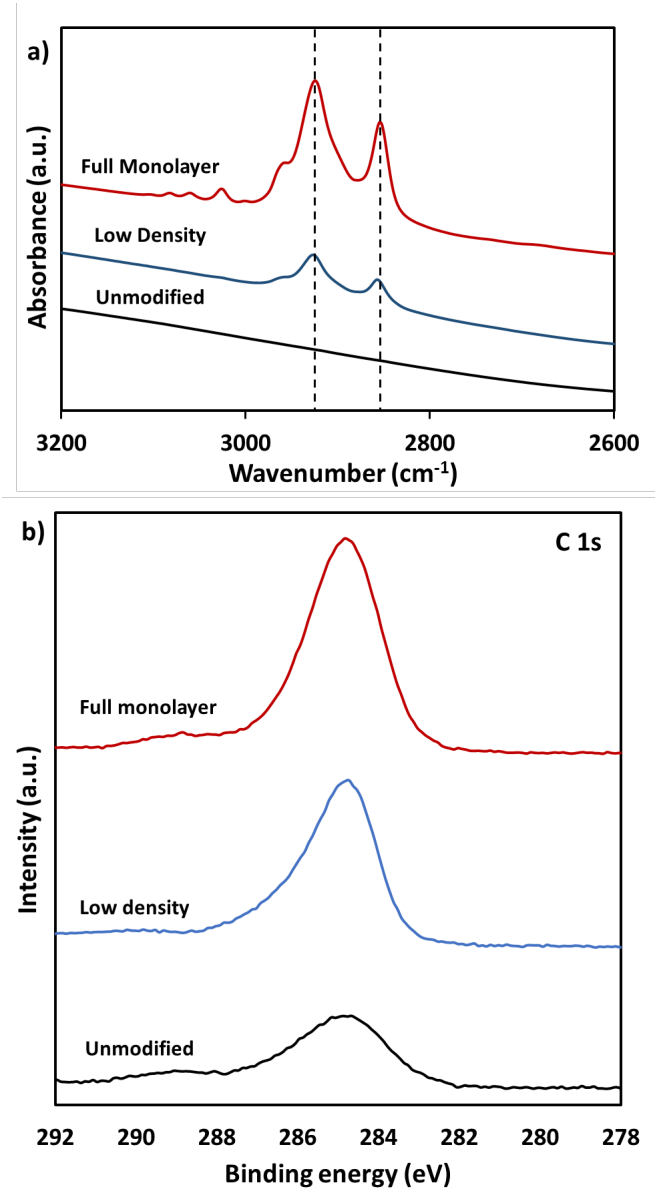

Figure 2. Catalyst characterization a) DRIFTS spectra for 5%Pt/Al_2O_3 (unmodified), LD-MHDA/5%Pt/Al_2O_3 (modified with low-density SAMs), and MHDA/5%Pt/Al_2O_3 (modified with full monolayer SAMs), and b) XPS analysis of 5%Pt/Al_2O_3 modified with MHDA monolayers focusing on the carbon 1s region.

TEM imaging was performed on three catalysts: 5%Pt/Al_2O_3, LD-MHDA/5%Pt/Al_2O_3, and MHDA/5%Pt/Al_2O_3 after pretreatment to ensure that the SAM modification did not affect Pt

particle size. Representative TEM images and particle size distributions are shown in Figure S4 and recorded in Table 1. The average particle sizes were found to be 6.2 ± 0.4 nm, 6.1 ± 0.5 nm, and 6.3 ± 0.3 nm for 5%Pt/Al_2O_3, LD-MHDA/5%Pt/Al_2O_3, and MHDA/5%Pt/Al_2O_3, respectively. Therefore, deposition of these SAMs had no observable effect on Pt particle size and differences observed in characterization and reaction data was not likely due to differences in particle size.

Catalysts were also characterized using CO chemisorption to determine the apparent dispersions (Table 1), which represent the fraction of available Pt sites. Deposition of a full monolayer of MHDA resulted in a decrease in apparent dispersion from 16.0% to 3.0%, indicating significant site-blocking (approximately 19% of sites were available i.e., 81% of sites were blocked) due to the high density of thiolates on the surface. Meanwhile, the apparent dispersion for LD-MHDA/5%Pt/Al_2O_3 was 12.2%, much closer to that of the unmodified case, suggesting that the Pt surface was significantly more available in the LD-monolayer case than with the full monolayer. Comparing this to the percentage of blocked sites found for MHDA/5%Pt/Al_2O_3, the low-density SAM blocked about 29% as many CO adsorption sites as the full monolayer. In other words, the low-density SAM had approximately 29% of the density of a full monolayer. Luo et al. reported densities of 55-60% of a full monolayer for LD-SAMs on flat Au surfaces.[35,36] The difference in relative density is likely because SAMs formation is dependent on the metal used (Au vs. Pt) and the curvature of the surface (flat 2D planes vs. nanoparticles).[28,43]

Catalysts were also characterized using ICP-OES to determine Pt and S loadings (Table S2). Sulfur was clearly abundant on both modified samples and absent on the 5%Pt/Al_2O_3, as expected. The fraction of Pt in the sample decreased after SAM deposition due to a larger fraction of the sample's mass coming from the MHDA. A sulfur loading of 0.24 wt% was found on LD-MHDA/5%Pt/Al_2O_3 while a much higher loading, 0.67 wt%, was found on MHDA/5%Pt/Al_2O_3.

However, ICP performed on bare Al_2O_3 that underwent the thiol deposition procedure revealed the presence of sulfur, indicating that the thiol SAMs may not be restricted solely to the Pt nanoparticles. Since it is unclear if the SAMs are uniformly decorating both Pt and Al_2O_3 (i.e., if SAM density would be the same on Al_2O_3 vs. Pt/Al_2O_3), ICP results were not used to quantitatively calculate SAM densities on the metal. Nevertheless, the lower sulfur loading found for LD-MHDA/5%Pt/Al_2O_3 suggested lower density on the low-density SAM and is consistent with the more quantitative results from CO chemisorption. Potassium content was also examined with ICP-OES. The last step in the low-density SAM synthesis involved ion exchange with $KClO_4$, so one might expect the terminal group of the ligands to contain potassium. However, negligible amounts (<0.05 wt%) were found in the samples with no apparent differences between the catalysts, indicating that potassium was removed at some point during the washing or reduction steps. Figure S5 shows DRIFT spectra in the characteristic carboxyl region. Characteristic asymmetric and symmetric COO stretching peaks for a carboxylate group coordinated with potassium are expected at approximately 1532 cm^{-1} and 1348 cm^{-1} respectively.[44] These were not observed for LD-MHDA/5%Pt/Al_2O_3. Additionally, the peaks for both modified samples were closely aligned with the expected peak positions for MHDA (~1574 cm^{-1} and ~1444 cm^{-1}).[45] This further indicated that the potassium was removed.

Table 1. Apparent dispersions determined using CO chemisorption, percent of sites available compared to unmodified 5%Pt/Al_2O_3 calculated using the dispersion ratios, and average particle sizes obtained from TEM.

Sample	Apparent Dispersion (%)	Percent of sites available compared to unmodified catalyst	Average particle size (nm) from TEM
5%Pt/Al_2O_3	16.0 ± 2.1	100	6.2 ± 0.4
LD-MHDA/5%Pt/Al_2O_3	12.2 ± 1.7	76 ± 15	6.1 ± 0.5
MHDA/5%Pt/Al_2O_3	3.0 ± 0.6	19 ± 4	6.3 ± 0.3

XPS was performed on all three catalysts, probing the C 1s (Figure 2b), Pt 4d, Pt 4f, N 1s, and O 1s regions (Figure S3). Pt 4d, Pt 4f, and O 1s binding energy peak locations are tabulated in Table S3. A clear trend in the magnitude of C 1s spectra was observed. The intensity of the peaks, representative of the amount of carbon on the surface, followed the trend of full monolayer > low-density SAM > unmodified 5%Pt/Al_2O_3. As expected, deposition of the SAM increased carbon content and LD-MHDA/5%Pt/Al_2O_3 had less carbon than the full monolayer. This provided additional qualitative confirmation that low-density SAMs had been formed. Additionally, the lack of signal in the N 1s region suggested that the final ion removal step during synthesis of the low-density SAM was successful and TEA was sufficiently removed from the sample.

Finally, DRIFT spectra were obtained after dosing CO on the samples to provide information on differences adsorption geometries. Figure 3 shows the IR region associated with CO adsorption on Pt. The spectrum from the unmodified catalyst contains a sharp peak at 2083 cm^{-1}, a shoulder at 2052 cm^{-1}, and a broad peak at 1837 cm^{-1}. The peak at 2083 cm^{-1} represents CO linearly bound to well-coordinated sites.[39,46,47] The shoulder at 2052 cm^{-1} represents CO linearly bound to undercoordinated sites and the peak at 1837 cm^{-1} indicates bridged CO binding.[39,46,47] Significant differences in the spectra were seen for MHDA/5%Pt/Al_2O_3. Only one peak at 2064 cm^{-1} was

observed for linearly bound CO. This suggested that all Pt sites available for CO linear binding were virtually the same. A reduction in peak intensity for bridge bound CO was observed as a result of thiolates obstructing contiguous Pt sites. The spectrum for LD-MHDA/5%Pt/Al_2O_3 was similar to that of the full monolayer, exhibiting only one peak for linearly bound CO and a reduction in bridge-bound CO. This provided evidence that ligands were well-dispersed across Pt (i.e., that the low-density SAM layer was homogeneous). If islanding/phase segregation were occurring, we would expect to see CO DRIFTS peak locations similar to that of the unmodified catalyst, but with reduced intensities. The difference in peak location for linearly bound CO could depend on multiple factors including differences in CO coverage and electronic effects from the thiols.[48] The single peak likely reflects the convolution of the two expected peaks – one for well-coordinated sites and one for undercoordinated sites. As such, the peak for LD-MHDA/5%Pt/Al_2O_3 may be shifted to a higher wavenumber because of a larger abundance of well-coordinated sites. This could suggest that MHDA and the ion-pair MHDA used in LD-MHDA/5%Pt/Al_2O_3 synthesis preferentially decorated Pt on different facets. Specifically, it is reasonable to postulate that MHDA ligands had a relatively higher propensity to decorate well-coordinated sites.

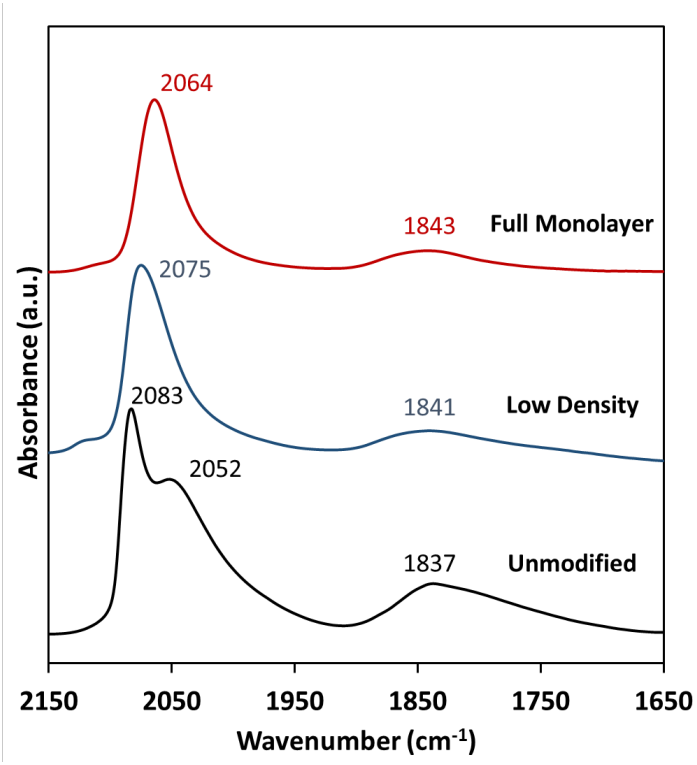

Figure 3. CO DRIFT spectra for 5%Pt/Al_2O_3 (unmodified), LD-MHDA/5%Pt/Al_2O_3 (modified with low-density SAMs), and MHDA/5%Pt/Al_2O_3 (modified with full monolayer SAMs) after dosing with CO for 20 min followed by purging with Ar for 20 min.

3.2 Effect of SAMs on Vapor Phase Benzyl Alcohol Hydrodeoxygenation

To determine the effect of MHDA monolayers on catalyst performance and the differences between the full monolayer and low-density SAM, gas-phase benzyl alcohol hydrodeoxygenation was performed. Pt/Al_2O_3 has been shown to be an effective catalyst for this reaction. While Pt is efficient for adsorbing and dissociating hydrogen, Al_2O_3 can provide acid sites that have been shown to promote HDO.[49–51] Activity results in the form of mass-normalized rates of product formation are shown in Figure 4. Selectivity to toluene, considered the desired product due to the importance of selectively removing oxygen from aromatic oxygenates in biomass upgrading,[52] is

also shown. The side product benzaldehyde was not included in selectivity calculations because prior work has shown that its formation is rapidly reversible under the reaction conditions and benzaldehyde yield drops to negligible levels at high benzyl alcohol conversion.[53]

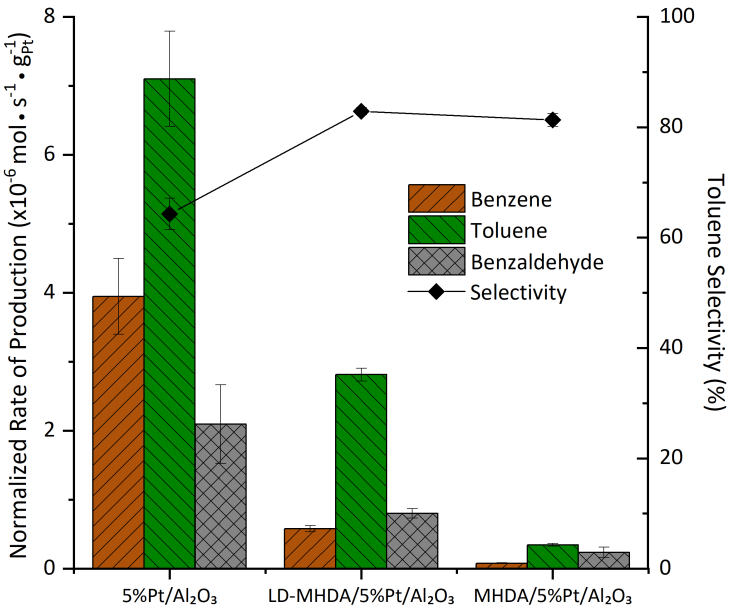

Figure 4. Gas-phase benzyl alcohol HDO performance over 5%Pt/Al_2O_3 modified with both low-density and a full monolayer of MHDA.

As hypothesized, MHDA/5%Pt/Al_2O_3 experienced a drastic reduction in activity relative to the unmodified catalyst. This was attributed to significant site-blocking that was apparent from the greatly reduced apparent dispersion from CO chemisorption experiments. Since acid sites on Al_2O_3 may provide a promotional effect for HDO,[49–51] site-blocking due to SAM coordination on the support may also decrease activity. However, an increase in toluene selectivity was observed. This likely resulted from the steric interactions between the ligands and the reactant. It has been shown that the different reaction pathways for benzyl alcohol hydrogenation are highly dependent on the

binding orientation of benzyl alcohol. In particular, for Pd catalysts, HDO has been proposed to occur via benzyl alcohol bound in an upright configuration; in contrast, if adsorption occurs through a flat-lying conformation, decarbonylation is more likely to occur.[54,55] Prior work done using high-resolution electron energy loss spectroscopy (HREELS) for benzyl alcohol adsorbed on single crystal Pd(111),[55] in-situ benzyl alcohol DRIFTS on Pd/Al_2O_3,[56] and in-situ furfural DRIFTS on Pd/Al_2O_3[57] have shown that thiol SAMs are capable of restricting binding orientation through an aromatic ring. To probe the binding orientation, DRIFT spectra, shown in Figure S6, were obtained after exposure to benzyl alcohol. For all samples, peaks were apparent at approximately 3070 cm^{-1} and 3030 cm^{-1}, representing C-H stretches of the aromatic ring, suggesting the presence of benzyl alcohol adsorbed on the surface.[58–61] Meanwhile, only the unmodified catalyst showed an increase in aliphatic C-H stretching between 2970 cm^{-1} and 2850 cm^{-1}. These stretches can be primarily attributed to benzyl alcohol that has reacted with hydrogen atoms from the decomposition of nearby adsorbates to generate a saturated ring.[57] This ring hydrogenation reaction pathway can occur if benzyl alcohol is adsorbed parallel to the catalyst surface. Since this was not seen for the thiol-modified catalysts, MHDA ligands likely inhibit benzyl alcohol coordinating through the aromatic ring. As a result, less decarbonylation occurs and toluene selectivity increases during benzyl alcohol hydrogenation over $MHDA/5\%Pt/Al_2O_3$. It has been previously suggested that thiols have a stronger poisoning effect on well-coordinated sites than on undercoordinated sites. This site-discrimination effect may also play a role in dictating reactant adsorption orientation as HDO is the prevailing reaction on undercoordinated sites.[56]

Similar improvements in toluene selectivity were found with $LD\text{-}MHDA/5\%Pt/Al_2O_3$. From this, it can be inferred that even with the lower MHDA coverage, the effective "gap" sizes between

ligands are small enough to restrict benzyl alcohol binding orientation. Meanwhile, LD-MHDA/5%Pt/Al_2O_3 was nearly an order of magnitude more active than MHDA/5%Pt/Al_2O_3. This is attributed to reduced site-blocking and an increased available "footprint" for benzyl alcohol adsorption. This is a major finding of the current work and highlights the potential advantages of low-density SAM modification of catalysts.

Using the apparent dispersions for each catalyst, apparent turnover frequencies (TOF) were calculated and are presented in Figure S7. These data suggest that some per-site activity is lost with the addition of ligands. This indicates that some sites on SAM-modified catalysts capable of CO chemisorption are less capable of benzyl alcohol HDO, consistent with the smaller size of CO compared to benzyl alcohol.

Time-on-stream data for benzyl alcohol hydrogenation is shown in Figure S8. In general, catalysts were fairly stable over the course of the reaction. While 5%Pt/Al_2O_3 and LD-MHDA/5%Pt/Al_2O_3 experienced slight losses in toluene production, the full monolayer did not. Thus, the full monolayer of MHDA may provide some stability benefits. This has been observed in SAM-modified catalysts in which SAMs increased catalyst stability by reducing sintering and the production of unwanted poisoning species derived from aromatics.[62]

3.3 Effect of SAMs on Liquid Phase Reactions

To explore the different effects of MHDA on catalysts in different reaction environments, liquid-phase reactions were performed. In addition to the different phase used, several other changes to reaction parameters should be noted compared to the gas-phase reactions described above. For example, the reactions were performed at significantly lower temperatures and higher hydrogen pressures. Figure 5 shows results for liquid-phase benzyl alcohol hydrogenation. Interestingly,

different products are observed compared to the gas-phase reactions. In the gas-phase reactions, decarbonylation was observed as a major reaction pathway. Under the liquid-phase reaction conditions, decarbonylation was not observed and instead ring hydrogenation to produce cyclohexylmethanol was a major reaction pathway. However, under both conditions HDO was a major pathway with significant toluene produced.

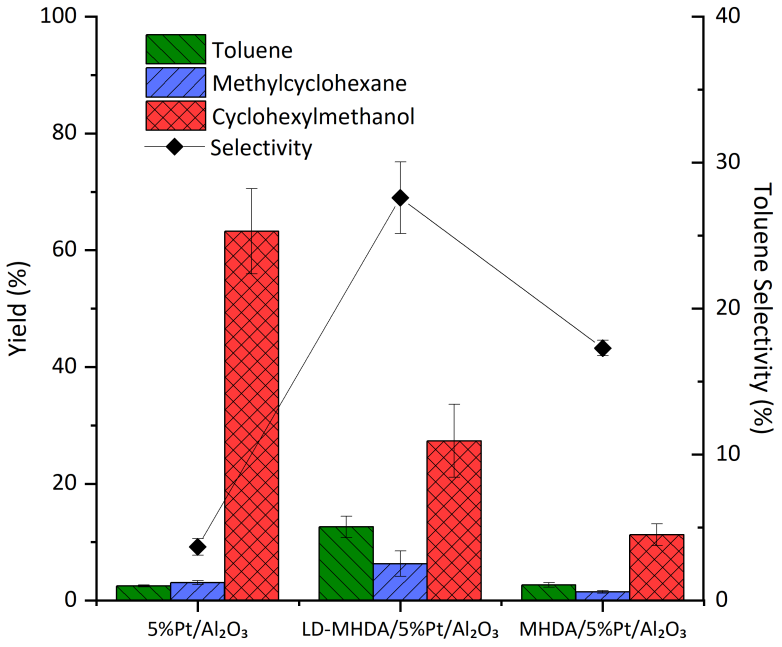

Figure 5. Liquid-phase benzyl alcohol hydrogenation performance over 5%Pt/Al_2O_3 modified with both low-density and a full monolayer of MHDA.

Several trends observed for the vapor phase reaction were preserved under the liquid-phase conditions. The trend in overall yield was unmodified > low-density SAM > full monolayer, consistent with gas-phase hydrogenation. In terms of overall yield, there was a strong correlation between activity and surface site availability. Comparing the apparent dispersion of SAM-modified catalysts and 5%Pt/Al_2O_3 (Table 1), the low-density SAM had approximately 76% of the

number of available sites compared to the unmodified catalyst, while the full monolayer retained only 19% of the available sites. Meanwhile, LD-MHDA/5%Pt/Al_2O_3 and MHDA/5%Pt/Al_2O_3 gave overall yields that were 67% and 22% of the yield obtained for 5%Pt/Al_2O_3, respectively.

Furthermore, focusing first on MHDA/5%Pt/Al_2O_3, it is important to note that almost all the activity loss was in the ring hydrogenation pathway. Roughly the same yield of toluene was found between 5%Pt/Al_2O_3 and MHDA/5%Pt/Al_2O_3. This resulted in a large increase in toluene selectivity from 3.7% to 17.3% - nearly five times more selective. The reduction in ring hydrogenation has previously been observed for thiol-modified Pd catalysts in which ring hydrogenation of furfural was suppressed.[63] Again, the suppression of ring hydrogenation likely occurred due to the ligands blocking the ability for the reactant to adsorb in a flat-lying conformation with the ring parallel to the surface. In fact, it is well-established that the preferential binding mode for the adsorption of aromatic compounds on Pt is through the pi system of the aromatic ring centered over a hollow site which allows for full ring hydrogenation.[64,65] Even though ring hydrogenation was greatly reduced for the SAM-modified catalyst, it was still a significant reaction pathway. While flat-lying adsorption is restricted by the thiol ligands, the existence of some contiguous unmodified Pt atoms is likely to exist. Specifically, even though the bridge-bound CO peak in the CO DRIFTS data in Figure 3 is small, we cannot rule out the possibility that there are inherent defects in the SAM layer or that thiol mobility under the reaction conditions may result in the existence of defects in the monolayer. This dynamic nature has been previously observed on Pt/Al_2O_3 catalysts under hydrogen-rich conditions.[66]

LD-MHDA/5%Pt/Al_2O_3 also experienced a large reduction in ring hydrogenation and increase in toluene selectivity. This reinforces the idea that the gaps in the low-density SAM can restrict the binding orientation similarly to the full monolayer. Interestingly, greater toluene selectivity,

27.6%, was found for LD-MHDA/5%Pt/Al_2O_3 compared to even MHDA/5%Pt/Al_2O_3. The decreased ring hydrogenation was accompanied by an increase in the production of toluene and methylcyclohexane. This suggested the potential presence of a promotional effect. To test this, 5%Pt/Al_2O_3 and LD-MHDA/5%Pt/Al_2O_3 were tested for benzyl alcohol hydrogenation again at similar, differential conversions and the selectivity and per-site activity (TOF) were analyzed.

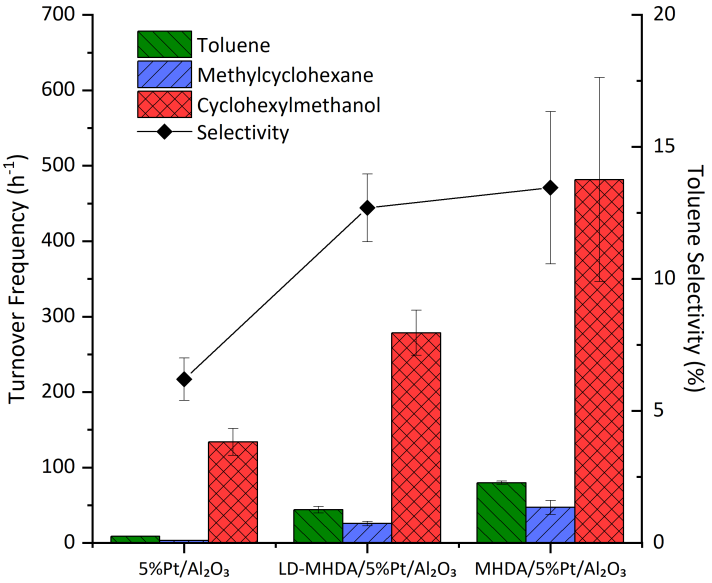

Figure 6. Liquid-phase benzyl alcohol hydrogenation performance at low conversion (~5%) normalized per active site (TOF).

Shown in Figure 6, the catalyst loading was controlled to achieve approximately 5% conversion. At these conditions, one would not expect significant changes in concentration profile over the course of the reaction. SAM-modified catalysts still exhibited improved toluene and methylcyclohexane activity and selectivity. Additionally, it was interesting that the activity normalized per active site (TOF) was higher for all products, even cyclohexylmethanol. This suggested the presence of a promotional effect from MHDA.

It is possible that the MHDA ligands may cause an electronic effect on Pt, as thiol coatings have been shown to affect Pt binding energies.[67] If there were electron transfer from Pt to sulfur, it would affect the binding strength of benzyl alcohol and products on Pt, which could explain the changes. Slight shifts in O 1s and Pt 4f binding energies for LD-MHDA/5%Pt/Al_2O_3 can be seen in Figure S3 and Table S3. It has been suggested that the Pt 4f binding energy should not be used for evaluation of electronic effects due to the overlap with the Al 2p region from the Al_2O_3 support.[68,69] Meanwhile, analysis of Pt 4d binding energy showed a shift of ~0.2 eV and was within the calculated error shown in Table S3. Thus, it is possible that there are minor electronic effects for LD-MHDA/5%Pt/Al_2O_3 but it is unlikely that these effects have a major role in the catalyst performance because these shifts were not observed for the full monolayer catalyst, which has even higher TOFs.

Another possibility is that under the reaction conditions used, the catalyst surface may become crowded with strongly bound aromatic intermediates and the ligands help prevent this accumulation.[53] Also, it is interesting that MHDA/5%Pt/Al_2O_3 provides greater site-normalized activity than LD-MHDA/5%Pt/Al_2O_3 indicating that the thiol density plays a role in promoting the reaction. Differences in ligand coverage have been shown to provide different levels of site modification for phosphonic acid-modified Pd/Al_2O_3 catalysts.[23]

Shown in Figure 7, liquid-phase hydrogenation was also performed using 2-phenyl-2-butanol as the reactant. This molecule is analogous to benzyl alcohol; however, the alcohol group is more sterically hindered. Similar to benzyl alcohol hydrogenation, an increase in HDO (sec-butylbenzene) selectivity was observed for the SAM-modified catalysts. Also as with benzyl alcohol, MHDA/5%Pt/Al_2O_3 saw an improvement in selectivity due to a reduction in the ring hydrogenation pathway producing 2-cyclohexyl-2-butanol. Meanwhile, HDO yield was not

decreased by a significant amount. LD-MHDA/5%Pt/Al_2O_3 similarly saw an increase in HDO selectivity. In addition to reduced ring hydrogenation, an increase in HDO production rate was also seen when compared to the unmodified catalyst, as shown in Figure 8a. Additional reactions were conducted controlling the catalyst loading to achieve low (~5%) conversions in order to analyze catalyst performance at differential conversion. Turnover frequencies (TOF) are shown in Figure S9. Both modified catalysts exhibited greater TOF for HDO when compared to the unmodified catalyst, with larger TOF observed for the full monolayer compared to the low-density SAM catalyst. This again suggests that the ligands were capable of influencing the reaction through multiple mechanisms.

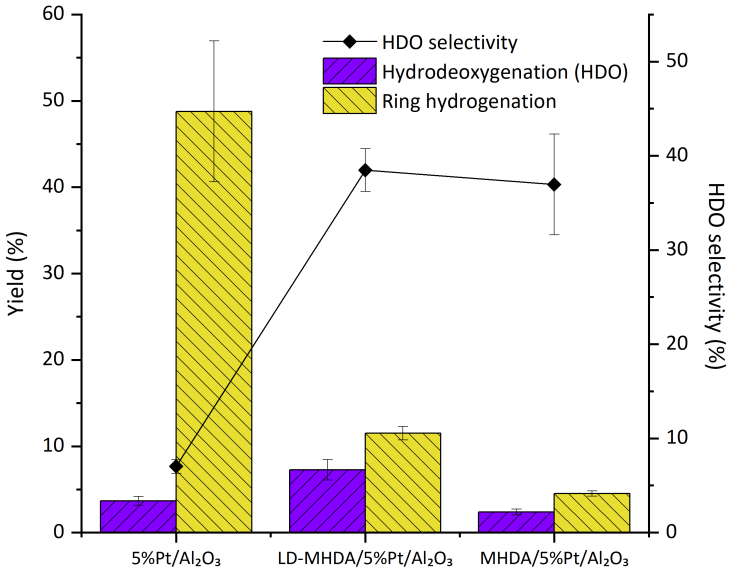

Figure 7. 2-phenyl-2-butanol hydrogenation reaction data over 5%Pt/Al_2O_3 modified with both low-density and a full monolayer of MHDA. The HDO and ring hydrogenation products are sec-butylbenzene and 2-cyclohexyl-2-butanol, respectively.

The trends in yield for 2-phenyl-2-butanol (Figure 7) were again similar to benzyl alcohol: unmodified > low-density SAM > full monolayer. However, an interesting observation can be made when focusing on the magnitude in activity loss (i.e., the decrease in total yield for a modified catalyst compared to the unmodified catalyst) due to the SAMs for the different reactants. When 2-phenyl-2-butanol was used as a reactant, the low-density SAM was more detrimental to overall activity. In this case, LD-MHDA/5%Pt/Al_2O_3 retained only ~36% activity. However, the loss in activity was attributed primarily to loss in the ring hydrogenation pathway as shown in Figure 8b. The greater decrease in activity was likely related to the size and bulkiness of the reactant compared to the gaps in the monolayer. This suggests that increasing SAM density affected ring hydrogenation and HDO in different ways, potentially providing a lever for controlling selectivity between the two pathways. This also indicated that the site requirements are markedly different.

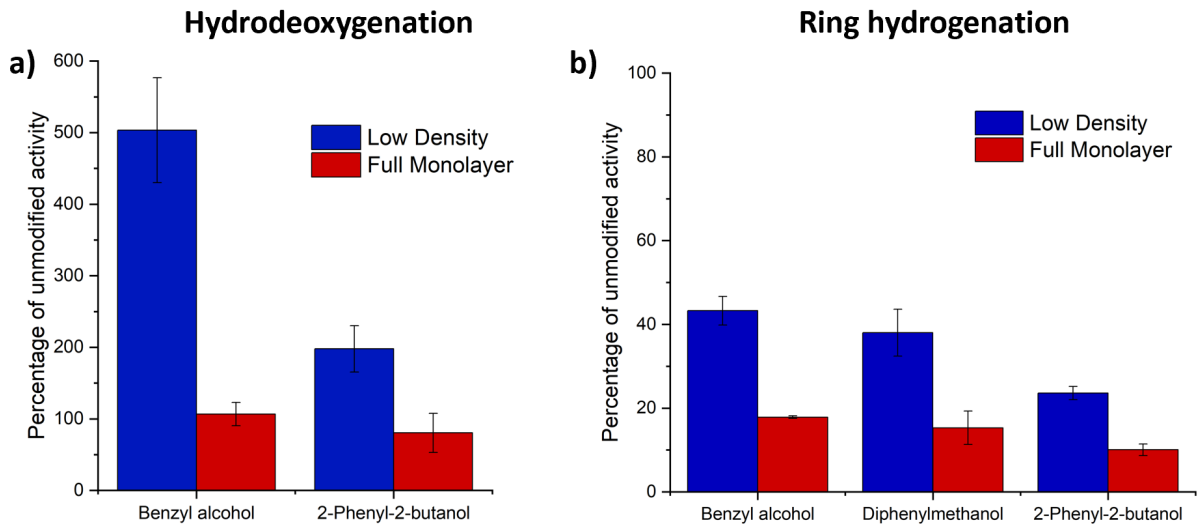

Figure 8. Performance of a) hydrodeoxygenation and b) ring hydrogenation reaction pathways for SAM-modified catalysts compared to unmodified 5%Pt/Al_2O_3. The majority of lost activity comes from ring hydrogenation. In fact, the low-density SAM gave significantly higher HDO yields than 5%Pt/Al_2O_3.

To further explore the relationship between reactant size and SAM density, another larger reactant, diphenylmethanol, was tested. Hydrogenation reaction data is shown in Figure S10. The overall yield includes both ring hydrogenation products, cyclohexylphenyl methanol and dicyclohexylmethanol. Meanwhile, no HDO products were observed for this reaction on any catalyst, consistent with observations in other work on hydrogenation of benzophenone and diphenylmethanol under similar reaction conditions.[70] As a result, these reaction data could only be used to study the effect on ring hydrogenation. In this case, LD-MHDA/5%Pt/Al_2O_3 retained ~38% activity compared to ~15% for MHDA/5%Pt/Al_2O_3. It is interesting that these results were very similar to those obtained with 2-phenyl-2-butanol, which retained ~34% and ~14% of the total yield, potentially suggesting that these two reactants had a similar "footprint" and therefore

experienced similar steric effects based on the size of the gaps in the SAM. However, HDO is not negatively affected by SAM density and the loss in activity was solely due to reduced ring hydrogenation. When focusing on 2-phenyl-2-butanol ring hydrogenation, LD-MHDA/5%Pt/Al_2O_3 and MHDA/5%Pt/Al_2O_3 retained only ~24% and ~10% of the yield of the unmodified catalyst. This would suggest that 2-phenyl-2-butanol is more affected by the SAMs than diphenylmethanol. This may be related to the bulkiness of the reactant (i.e., the planar configuration of diphenylmethanol is less of a hinderance).

Clearly, the effect of SAM density on catalyst performance is a complex phenomenon depending on multiple factors including the size and bulkiness of the reactant as well as the specific reaction pathway. Site blocking with thiols was shown to be beneficial in improving HDO activity, with reduced density promoting activity to a large extent. That is, the low-density SAM appeared to achieve the beneficial effects of the modifier for active site modification without the excessive site blocking associated with full coverage. Meanwhile, SAM density greatly diminished ring hydrogenation.

4. Conclusions

Pt/Al_2O_3 was modified with a full thiol monolayer and a low-density thiol monolayer to explore the effect of ligand density on activity and selectivity for hydrogenation reactions. First, the synthesis procedure used to deposit the low-density SAM was found to be successful and homogeneous low-density SAMs were reliably formed having ~1/3rd the coverage of the full monolayer, blocking significantly less Pt sites. Reactions of gas-phase and liquid-phase benzyl alcohol hydrogenation were shown to significantly improve HDO selectivity by suppressing decarbonylation and ring hydrogenation reaction pathways. This was attributed to ligands controlling the binding orientation of benzyl alcohol. The low-density SAM catalyst retained

selectivity benefits while greatly restoring activity due to reduced site-blocking. Reactants with differences in size and bulkiness were also tested and a correlation was found between the size of reactant and how influential the SAMs were on activity. All reactants experienced large decreases in ring hydrogenation. However, HDO yields actually increased with the low-density SAM modified catalyst, although providing lesser improvement for the larger 2-phenyl-2-butanol reactant. As SAM density affected separate reaction pathways differently, this allowed for control of HDO selectivity. The low-density SAM in this work was effective for promoting benzyl alcohol HDO, but presumably SAM density and gap size could be tailored for other reactions.

ASSOCIATED CONTENT

Supporting Information.

The Supporting Information are available free of charge.

Supporting information includes additional characterization and reaction data as mentioned in the text (DOC).

AUTHOR INFORMATION

Corresponding Author

*E-mail: Will.Medlin@colorado.edu

Author Contributions

The manuscript was written through contributions of all authors. All authors have given approval to the final version of the manuscript.

Funding Sources

This research was supported by the National Science Foundation [grant no. 2004090].

Notes

The authors report no competing financial interest.

ACKNOWLEDGMENT

The authors acknowledge Xinpei Zhou, Erin Dunphy, and Ezra Baghdady for help with CO chemisorption, XPS, and TEM experiments.

REFERENCES

(1) Cole-Hamilton, D. J. Homogeneous Catalysis--New Approaches to Catalyst Separation, Recovery, and Recycling. *Science* **2003**, *299* (5613), 1702–1706. https://doi.org/10.1126/science.1081881.

(2) Cui, X.; Li, W.; Ryabchuk, P.; Junge, K.; Beller, M. Bridging Homogeneous and Heterogeneous Catalysis by Heterogeneous Single-Metal-Site Catalysts. *Nat Catal* **2018**, *1* (6), 385–397. https://doi.org/10.1038/s41929-018-0090-9.

(3) Chia, M.; Pagán-Torres, Y. J.; Hibbitts, D.; Tan, Q.; Pham, H. N.; Datye, A. K.; Neurock, M.; Davis, R. J.; Dumesic, J. A. Selective Hydrogenolysis of Polyols and Cyclic Ethers over Bifunctional Surface Sites on Rhodium–Rhenium Catalysts. *J. Am. Chem. Soc.* **2011**, *133* (32), 12675–12689. https://doi.org/10.1021/ja2038358.

(4) Do, P. T. M.; Foster, A. J.; Chen, J.; Lobo, R. F. Bimetallic Effects in the Hydrodeoxygenation of Meta-Cresol on γ-Al2O3 Supported Pt–Ni and Pt–Co Catalysts. *Green Chem.* **2012**, *14* (5), 1388. https://doi.org/10.1039/c2gc16544a.

(5) Van Santen, R. A. Complementary Structure Sensitive and Insensitive Catalytic Relationships. *Acc. Chem. Res.* **2009**, *42* (1), 57–66. https://doi.org/10.1021/ar800022m.

(6) Yu, Z.; Lu, X.; Wang, X.; Xiong, J.; Li, X.; Zhang, R.; Ji, N. Metal-Catalyzed Hydrogenation of Biomass-Derived Furfural: Particle Size Effects and Regulation Strategies. *ChemSusChem* **2020**, *13* (19), 5185–5198. https://doi.org/10.1002/cssc.202001467.

(7) Ponec, V. Alloy Catalysts: The Concepts. *Applied Catalysis A: General* **2001**, *222* (1–2), 31–45. https://doi.org/10.1016/S0926-860X(01)00828-6.

(8) Zhang, T.; Walsh, A. G.; Yu, J.; Zhang, P. Single-Atom Alloy Catalysts: Structural Analysis, Electronic Properties and Catalytic Activities. *Chem. Soc. Rev.* **2021**, *50* (1), 569–588. https://doi.org/10.1039/D0CS00844C.

(9) Vargas, K. M.; San, K. A.; Shon, Y.-S. Isolated Effects of Surface Ligand Density on the Catalytic Activity and Selectivity of Palladium Nanoparticles. *ACS Appl. Nano Mater.* **2019**, *2* (11), 7188–7196. https://doi.org/10.1021/acsanm.9b01696.

(10) Gavia, D. J.; Shon, Y.-S. Controlling Surface Ligand Density and Core Size of Alkanethiolate-Capped Pd Nanoparticles and Their Effects on Catalysis. *Langmuir* **2012**, *28* (40), 14502–14508. https://doi.org/10.1021/la302653u.

(11) Paz Herrera, L.; Freitas de Lima e Freitas, L.; Hong, J.; Hoffman, A. S.; Bare, S. R.; Nikolla, E.; Medlin, J. W. Reactivity of Pd–MO_2 Encapsulated Catalytic Systems for CO Oxidation. *Catal. Sci. Technol.* **2022**, *12* (5), 1476–1486. https://doi.org/10.1039/D1CY01916C.

(12) Chen, G.; Xu, C.; Huang, X.; Ye, J.; Gu, L.; Li, G.; Tang, Z.; Wu, B.; Yang, H.; Zhao, Z.; Zhou, Z.; Fu, G.; Zheng, N. Interfacial Electronic Effects Control the Reaction Selectivity of Platinum Catalysts. *Nature Mater* **2016**, *15* (5), 564–569. https://doi.org/10.1038/nmat4555.

(13) Chatterjee, P.; Wang, H.; Manzano, J. S.; Kanbur, U.; Sadow, A. D.; Slowing, I. I. Surface Ligands Enhance the Catalytic Activity of Supported Au Nanoparticles for the Aerobic α-Oxidation of Amines to Amides. *Catal. Sci. Technol.* **2022**, *12* (6), 1922–1933. https://doi.org/10.1039/D1CY02121D.

(14) Zhang, J.; Ellis, L. D.; Wang, B.; Dzara, M. J.; Sievers, C.; Pylypenko, S.; Nikolla, E.; Medlin, J. W. Control of Interfacial Acid–Metal Catalysis with Organic Monolayers. *Nat Catal* **2018**, *1* (2), 148–155. https://doi.org/10.1038/s41929-017-0019-8.

(15) Zhang, J.; Deo, S.; Janik, M. J.; Medlin, J. W. Control of Molecular Bonding Strength on Metal Catalysts with Organic Monolayers for CO2 Reduction. *J. Am. Chem. Soc.* **2020**, jacs.9b12980. https://doi.org/10.1021/jacs.9b12980.
(16) Taguchi, T.; Isozaki, K.; Miki, K. Enhanced Catalytic Activity of Self-Assembled-Monolayer-Capped Gold Nanoparticles. *Adv. Mater.* **2012**, *24* (48), 6462–6467. https://doi.org/10.1002/adma.201202979.
(17) Kahsar, K. R.; Schwartz, D. K.; Medlin, J. W. Control of Metal Catalyst Selectivity through Specific Noncovalent Molecular Interactions. *J. Am. Chem. Soc.* **2014**, *136* (1), 520–526. https://doi.org/10.1021/ja411973p.
(18) Pecsi, I.; Leveles, I.; Harmat, V.; Vertessy, B. G.; Toth, J. Aromatic Stacking between Nucleobase and Enzyme Promotes Phosphate Ester Hydrolysis in DUTPase. *Nucleic Acids Research* **2010**, *38* (20), 7179–7186. https://doi.org/10.1093/nar/gkq584.
(19) Chen, K.; Wu, H.; Hua, Q.; Chang, S.; Huang, W. Enhancing Catalytic Selectivity of Supported Metal Nanoparticles with Capping Ligands. *Phys. Chem. Chem. Phys.* **2013**, *15* (7), 2273. https://doi.org/10.1039/c2cp44571a.
(20) Campisi, S.; Ferri, D.; Villa, A.; Wang, W.; Wang, D.; Kröcher, O.; Prati, L. Selectivity Control in Palladium-Catalyzed Alcohol Oxidation through Selective Blocking of Active Sites. *J. Phys. Chem. C* **2016**, *120* (26), 14027–14033. https://doi.org/10.1021/acs.jpcc.6b01549.
(21) Wu, D.; Baaziz, W.; Gu, B.; Marinova, M.; Hernández, W. Y.; Zhou, W.; Vovk, E. I.; Ersen, O.; Safonova, O. V.; Addad, A.; Nuns, N.; Khodakov, A. Y.; Ordomsky, V. V. Surface Molecular Imprinting over Supported Metal Catalysts for Size-Dependent Selective Hydrogenation Reactions. *Nat Catal* **2021**, *4* (7), 595–606. https://doi.org/10.1038/s41929-021-00649-3.
(22) Ansar, S. M.; Kitchens, C. L. Impact of Gold Nanoparticle Stabilizing Ligands on the Colloidal Catalytic Reduction of 4-Nitrophenol. *ACS Catal.* **2016**, *6* (8), 5553–5560. https://doi.org/10.1021/acscatal.6b00635.
(23) Blanchette, Z.; Zhang, J.; Yazdi, S.; Griffin, M. B.; Schwartz, D. K.; Medlin, J. W. Investigating Deposition Sequence during Synthesis of Pd/Al $_2$ O $_3$ Catalysts Modified with Organic Monolayers. *Catal. Sci. Technol.* **2022**, *12* (7), 2306–2314. https://doi.org/10.1039/D1CY02131A.
(24) Slot, T. K.; Riley, N.; Shiju, N. R.; Medlin, J. W.; Rothenberg, G. An Experimental Approach for Controlling Confinement Effects at Catalyst Interfaces. *Chem. Sci.* **2020**, *11* (40), 11024–11029. https://doi.org/10.1039/D0SC04118A.
(25) Yoskamtorn, T.; Yamazoe, S.; Takahata, R.; Nishigaki, J.; Thivasasith, A.; Limtrakul, J.; Tsukuda, T. Thiolate-Mediated Selectivity Control in Aerobic Alcohol Oxidation by Porous Carbon-Supported Au $_{25}$ Clusters. *ACS Catal.* **2014**, *4* (10), 3696–3700. https://doi.org/10.1021/cs501010x.
(26) Lu, L.; Zou, S.; Zhou, Y.; Liu, J.; Li, R.; Xu, Z.; Xiao, L.; Fan, J. Ligand-Regulated ORR Activity of Au Nanoparticles in Alkaline Medium: The Importance of Surface Coverage of Ligands. *Catal. Sci. Technol.* **2018**, *8* (3), 746–754. https://doi.org/10.1039/C7CY02101A.
(27) Schwartz, D. K. MECHANISMS AND KINETICS OF SELF-ASSEMBLED MONOLAYER FORMATION. *Annu. Rev. Phys. Chem.* **2001**, *52* (1), 107–137. https://doi.org/10.1146/annurev.physchem.52.1.107.

(28) Love, J. C.; Estroff, L. A.; Kriebel, J. K.; Nuzzo, R. G.; Whitesides, G. M. Self-Assembled Monolayers of Thiolates on Metals as a Form of Nanotechnology. *Chem. Rev.* **2005**, *105* (4), 1103–1170. https://doi.org/10.1021/cr0300789.
(29) Besharat, Z.; Wakeham, D.; Johnson, C. M.; Luengo, G. S.; Greaves, A.; Odnevall Wallinder, I.; Göthelid, M.; Rutland, M. W. Mixed Monolayers of Alkane Thiols with Polar Terminal Group on Gold: Investigation of Structure Dependent Surface Properties. *Journal of Colloid and Interface Science* **2016**, *484*, 279–290. https://doi.org/10.1016/j.jcis.2016.08.053.
(30) Park, J.-S.; Vo, A. N.; Barriet, D.; Shon, Y.-S.; Lee, T. R. Systematic Control of the Packing Density of Self-Assembled Monolayers Using Bidentate and Tridentate Chelating Alkanethiols. *Langmuir* **2005**, *21* (7), 2902–2911. https://doi.org/10.1021/la0475573.
(31) Garg, N.; Friedman, J. M.; Lee, T. R. Adsorption Profiles of Chelating Aromatic Dithiols and Disulfides: Comparison to Those of Normal Alkanethiols and Disulfides. *Langmuir* **2000**, *16* (9), 4266–4271. https://doi.org/10.1021/la991100p.
(32) Lahann, J. A Reversibly Switching Surface. *Science* **2003**, *299* (5605), 371–374. https://doi.org/10.1126/science.1078933.
(33) Berron, B.; Jennings, G. K. Loosely Packed Hydroxyl-Terminated SAMs on Gold. *Langmuir* **2006**, *22* (17), 7235–7240. https://doi.org/10.1021/la0531650.
(34) Iqbal, P.; Rawson, F. J.; Ho, W. K.-W.; Lee, S.-F.; Leung, K. C.-F.; Wang, X.; Beri, A.; Preece, J. A.; Ma, J.; Mendes, P. M. Surface Molecular Tailoring Using PH-Switchable Supramolecular Dendron-Ligand Assemblies. *ACS Appl. Mater. Interfaces* **2014**, *6* (9), 6264–6274. https://doi.org/10.1021/am501613c.
(35) Olivier, G. K.; Shin, D.; Gilbert, J. B.; Monzon, L. M. A.; Frechette, J. Supramolecular Ion-Pair Interactions To Control Monolayer Assembly. *Langmuir* **2009**, *25* (4), 2159–2165. https://doi.org/10.1021/la803057x.
(36) Luo, M.; Frechette, J. Electrochemical Stability of Low-Density Carboxylic Acid Terminated Monolayers. *J. Phys. Chem. C* **2010**, *114* (47), 20167–20172. https://doi.org/10.1021/jp108018f.
(37) Luo, M.; Amegashie, A.; Chua, A.; Olivier, G. K.; Frechette, J. Role of Solution and Surface Coverage on Voltage-Induced Response of Low-Density Self-Assembled Monolayers. *J. Phys. Chem. C* **2012**, *116* (26), 13964–13971. https://doi.org/10.1021/jp3020996.
(38) Fortunato, M. A.; Aubert, D.; Capdeillayre, C.; Daniel, C.; Hadjar, A.; Princivalle, A.; Guizard, C.; Vernoux, P. Dispersion Measurement of Platinum Supported on Yttria-Stabilised Zirconia by Pulse H2 Chemisorption. *Applied Catalysis A: General* **2011**, *403* (1–2), 18–24. https://doi.org/10.1016/j.apcata.2011.06.005.
(39) Allian, A. D.; Takanabe, K.; Fujdala, K. L.; Hao, X.; Truex, T. J.; Cai, J.; Buda, C.; Neurock, M.; Iglesia, E. Chemisorption of CO and Mechanism of CO Oxidation on Supported Platinum Nanoclusters. *J. Am. Chem. Soc.* **2011**, *133* (12), 4498–4517. https://doi.org/10.1021/ja110073u.
(40) Safazadeh, L.; Berron, B. J. Photopatterning of Stable, Low-Density, Self-Assembled Monolayers on Gold. *Langmuir* **2015**, *31* (9), 2689–2696. https://doi.org/10.1021/acs.langmuir.5b00001.
(41) Peng, D. K.; Lahann, J. Chemical, Electrochemical, and Structural Stability of Low-Density Self-Assembled Monolayers. *Langmuir* **2007**, *23* (20), 10184–10189. https://doi.org/10.1021/la701607e.
(42) Vericat, C.; Vela, M. E.; Corthey, G.; Pensa, E.; Cortés, E.; Fonticelli, M. H.; Ibañez, F.; Benitez, G. E.; Carro, P.; Salvarezza, R. C. Self-Assembled Monolayers of Thiolates on

Metals: A Review Article on Sulfur-Metal Chemistry and Surface Structures. *RSC Adv.* **2014**, *4* (53), 27730–27754. https://doi.org/10.1039/C4RA04659E.
(43) Petrovykh, D. Y.; Kimura-Suda, H.; Opdahl, A.; Richter, L. J.; Tarlov, M. J.; Whitman, L. J. Alkanethiols on Platinum: Multicomponent Self-Assembled Monolayers. *Langmuir* **2006**, *22* (6), 2578–2587. https://doi.org/10.1021/la050928a.
(44) Ibrahim, M.; Nada, A.; Kamal, D. E. Density Functional Theory and FTIR Spectroscopic Study of Carboxyl Group. *APPL PHYS* **2005**, *43*.
(45) Myrskog, A.; Anderson, H.; Aastrup, T.; Ingemarsson, B.; Liedberg, B. Esterification of Self-Assembled Carboxylic-Acid-Terminated Thiol Monolayers in Acid Environment: A Time-Dependent Study. *Langmuir* **2010**, *26* (2), 821–829. https://doi.org/10.1021/la902255j.
(46) Kale, M. J.; Christopher, P. Utilizing Quantitative *in Situ* FTIR Spectroscopy To Identify Well-Coordinated Pt Atoms as the Active Site for CO Oxidation on Al_2O_3-Supported Pt Catalysts. *ACS Catal.* **2016**, *6* (8), 5599–5609. https://doi.org/10.1021/acscatal.6b01128.
(47) Fouladvand, S.; Skoglundh, M.; Carlsson, P.-A. A Transient *in Situ* Infrared Spectroscopy Study on Methane Oxidation over Supported Pt Catalysts. *Catal. Sci. Technol.* **2014**, *4* (10), 3463–3473. https://doi.org/10.1039/C4CY00486H.
(48) Stoop, F. Geometric and Ligand Effects in the Infrared Spectra of Adsorbed Carbon Monoxide. *Journal of Catalysis* **1982**, *73* (1), 50–56. https://doi.org/10.1016/0021-9517(82)90079-3.
(49) González, C.; Marín, P.; Díez, F. V.; Ordóñez, S. Gas-Phase Hydrodeoxygenation of Benzaldehyde, Benzyl Alcohol, Phenyl Acetate, and Anisole over Precious Metal Catalysts. *Ind. Eng. Chem. Res.* **2016**, *55* (8), 2319–2327. https://doi.org/10.1021/acs.iecr.6b00036.
(50) Faba, L.; Díaz, E.; Ordóñez, S. Hydrodeoxygenation of Acetone–Furfural Condensation Adducts over Alumina-Supported Noble Metal Catalysts. *Applied Catalysis B: Environmental* **2014**, *160–161*, 436–444. https://doi.org/10.1016/j.apcatb.2014.05.053.
(51) Foster, A. J.; Do, P. T. M.; Lobo, R. F. The Synergy of the Support Acid Function and the Metal Function in the Catalytic Hydrodeoxygenation of M-Cresol. *Top Catal* **2012**, *55* (3–4), 118–128. https://doi.org/10.1007/s11244-012-9781-7.
(52) Bridgwater, A. V. Review of Fast Pyrolysis of Biomass and Product Upgrading. *Biomass and Bioenergy* **2012**, *38*, 68–94. https://doi.org/10.1016/j.biombioe.2011.01.048.
(53) Lien, C.-H.; Medlin, J. W. Promotion of Activity and Selectivity by Alkanethiol Monolayers for Pd-Catalyzed Benzyl Alcohol Hydrodeoxygenation. *J. Phys. Chem. C* **2014**, *118* (41), 23783–23789. https://doi.org/10.1021/jp507114g.
(54) Zhang, J.; Wang, B.; Nikolla, E.; Medlin, J. W. Directing Reaction Pathways through Controlled Reactant Binding at Pd-TiO_2 Interfaces. *Angew. Chem. Int. Ed.* **2017**, *56* (23), 6594–6598. https://doi.org/10.1002/anie.201703669.
(55) Pang, S. H.; Roman, A. M.; Medlin, J. W. Adsorption Orientation-Induced Selectivity Control of Reactions of Benzyl Alcohol on Pd(111). *J. Phys. Chem. C* **2012**, 7.
(56) Lien, C.-H.; Medlin, J. W. Control of Pd Catalyst Selectivity with Mixed Thiolate Monolayers. *Journal of Catalysis* **2016**, *339*, 38–46. https://doi.org/10.1016/j.jcat.2016.04.001.
(57) Pang, S. H.; Schoenbaum, C. A.; Schwartz, D. K.; Medlin, J. W. Directing Reaction Pathways by Catalyst Active-Site Selection Using Self-Assembled Monolayers. *Nat Commun* **2013**, *4* (1), 2448. https://doi.org/10.1038/ncomms3448.

(58) Jentys, A.; Lercher, J. A. IR Study of The Adsorption of Benzene on HZSM5. In *Studies in Surface Science and Catalysis*; Elsevier, 1989; Vol. 46, pp 585–594. https://doi.org/10.1016/S0167-2991(08)61013-7.
(59) Armaroli, T.; Bevilacqua, M.; Trombetta, M.; Alejandre, A. G.; Ramirez, J.; Busca, G. An FT-IR Study of the Adsorption of Aromatic Hydrocarbons and of 2,6-Lutidine on H-FER and H-ZSM-5 Zeolites. *Applied Catalysis A: General* **2001**, *220* (1–2), 181–190. https://doi.org/10.1016/S0926-860X(01)00720-7.
(60) Qin, S.; Wang, J.; Zhao, C.; Zhang, S. Long-Term, Low Temperature Simulation of Early Diagenetic Alterations of Organic Matter: A FTIR Study. *Energy Exploration & Exploitation* **2010**, *28* (5), 365–376. https://doi.org/10.1260/0144-5987.28.5.365.
(61) Sandford, S. A.; Bernstein, M. P.; Materese, C. K. THE INFRARED SPECTRA OF POLYCYCLIC AROMATIC HYDROCARBONS WITH EXCESS PERIPHERAL H ATOMS (H $_n$ -PAHs) AND THEIR RELATION TO THE 3.4 AND 6.9 Mm PAH EMISSION FEATURES. *ApJS* **2013**, *205* (1), 8. https://doi.org/10.1088/0067-0049/205/1/8.
(62) Jenkins, A. H.; Musgrave, C. B.; Medlin, J. W. Enhancing Au/TiO $_2$ Catalyst Thermostability and Coking Resistance with Alkyl Phosphonic-Acid Self-Assembled Monolayers. *ACS Appl. Mater. Interfaces* **2019**, *11* (44), 41289–41296. https://doi.org/10.1021/acsami.9b13170.
(63) Coan, P. D.; Farberow, C. A.; Griffin, M. B.; Medlin, J. W. Organic Modifiers Promote Furfuryl Alcohol Ring Hydrogenation via Surface Hydrogen-Bonding Interactions. *ACS Catal.* **2021**, *11* (6), 3730–3739. https://doi.org/10.1021/acscatal.0c04138.
(64) Vorotnikov, V.; Mpourmpakis, G.; Vlachos, D. G. DFT Study of Furfural Conversion to Furan, Furfuryl Alcohol, and 2-Methylfuran on Pd(111). *ACS Catal.* **2012**, *2* (12), 2496–2504. https://doi.org/10.1021/cs300395a.
(65) Rodríguez, J. L.; Pastor, E. A Comparative Study on the Adsorption of Benzyl Alcohol, Toluene and Benzene on Platinum. *Electrochimica Acta* **2000**, *45* (25–26), 4279–4289. https://doi.org/10.1016/S0013-4686(00)00561-2.
(66) Corpuz, A. R.; Pang, S. H.; Schoenbaum, C. A.; Medlin, J. W. Hydrogen Exposure Effects on Pt/Al $_2$ O $_3$ Catalysts Coated with Thiolate Monolayers. *Langmuir* **2014**, *30* (46), 14104–14110. https://doi.org/10.1021/la503291y.
(67) Dablemont, C.; Lang, P.; Mangeney, C.; Piquemal, J.-Y.; Petkov, V.; Herbst, F.; Viau, G. FTIR and XPS Study of Pt Nanoparticle Functionalization and Interaction with Alumina. *Langmuir* **2008**, *24* (11), 5832–5841. https://doi.org/10.1021/la7028643.
(68) Shyu, J. Z.; Otto, K. IDENTIFICATION OF PLATINUM PHASES ON γ-ALUMINA BY XPS. *Applied Surface Science* **1988**, *32* (1–2), 246–252. https://doi.org/10.1016/0169-4332(88)90085-2.
(69) Pérez-Bustos, H. F.; Lucio-Ortiz, C. J.; De La Rosa, J. R.; De Haro Del Río, D. A.; Sandoval-Rangel, L.; Martínez-Vargas, D. X.; Maldonado, C. S.; Rodriguez-González, V.; Garza-Navarro, M. A.; Morales-Leal, F. J. Synthesis and Characterization of Bimetallic Catalysts Pd-Ru and Pt-Ru Supported on γ-Alumina and Zeolite FAU for the Catalytic Transformation of HMF. *Fuel* **2019**, *239*, 191–201. https://doi.org/10.1016/j.fuel.2018.10.001.
(70) Santori, G. F.; Moglioni, A. G.; Vetere, V.; Iglesias, G. Y. M.; Casella, M. L.; Ferretti, O. A. Hydrogenation of Aromatic Ketones with Pt- and Sn-Modified Pt Catalysts. *Applied Catalysis A: General* **2004**, *269* (1–2), 215–223. https://doi.org/10.1016/j.apcata.2004.04.020.

For Table of Contents Only